

Spatial extent of fragment-ion abundances in electron transfer dissociation and electron capture dissociation mass spectrometry of peptides

Jack Simons^{a,*}, Aaron R. Ledvina^b

^a Chemistry Department and Henry Eyring Center for Theoretical Chemistry, University of Utah, Salt Lake City, UT 84112, USA

^b Departments of Chemistry and Biomolecular Chemistry, University of Wisconsin, Madison, WI 53706, USA

ARTICLE INFO

Article history:

Received 19 April 2012

Received in revised form 17 July 2012

Accepted 17 July 2012

Available online 4 August 2012

Keywords:

Electron transfer dissociation

Electron capture dissociation

Fragmentation patterns

ABSTRACT

Earlier work from the first author's group has suggested that, in electron capture dissociation (ECD) or electron transfer dissociation (ETD) mass spectrometry experiments, an electron is initially attached into a Rydberg orbital centered at one of the peptide's positive sites (likely a protonated N-terminus, Lysine, Arginine, or Histidine). Moreover, this earlier work predicted that only Rydberg orbitals having principal quantum numbers $n=3-6$ are populated in ECD and only $n=3$ and 4 in ETD (when an anion donor having an electron binding energy of ca. 0.6 eV is used), and that the populations of these levels are very similar in the nascent charge-reduced peptide. Based upon these predictions, the present paper develops a framework for predicting the abundances of closed-shell c and open-shell z^* fragments as a function of distance along the backbone from the site initially holding the attached electron in a Rydberg orbital. The framework is not aimed at differences in branching ratios caused by differences in the physical properties of side chains along the backbone but on the spatial distances between the charged site holding the electron and the backbone amide units. The predictions of this model are tested using ECD and ETD data from derived from experiments carried out using simultaneous infrared photo-activation of the parent ions. Such activated-ion (AI) experiments are thought to disrupt much of the parent ion's secondary structure, which we believe allows us to make more reliable estimates of distances between the charged sites and the various amino acids' amide groups. The abundance patterns predicted based upon the framework described herein are found to be reasonably consistent with the experimental data. However, the data also provide evidence that internal solvation of the peptide's charged sites remains intact even under AI conditions, and that some of these solvated-ion structures (those involving a charged Lys or N-terminal amine) contribute incrementally to the abundances of fragment ions arising from cleaving nearby $N-C_{\alpha}$ bonds. As a result, we conclude that ECD and ETD fragment ion abundances are determined by a combination of factors: (i) internal solvation of charged sites, (ii) spatial distributions or Rydberg orbitals charge densities within several residues of charged sites, and (iii) variations induced by differences in physical properties of side chains. It is primarily the first two of these three that the present paper addresses.

© 2012 Elsevier B.V. All rights reserved.

1. Introduction

In electron-transfer dissociation [1–5] (ETD) or in electron-capture dissociation [6–9] (ECD) mass spectrometry experiments, an electron attaches to a multiply positively charged gas-phase peptide and induces bond cleavages within the charge-reduced peptide. ECD and ETD are relatively new yet extremely promising analytical techniques that are found to generate significantly higher backbone cleavage fractions than collisional or infrared dissociation techniques, while doing so with great specificity (i.e., in peptides, primarily $N-C_{\alpha}$ and $S-S$ bonds are cleaved) and leaving

post translational modifications intact to a great extent. Why $N-C_{\alpha}$ and $S-S$ bonds cleave and why they do throughout such a large fraction of the backbone need to be explained, and this has been the focus of much of the theoretical work in this area.

In earlier research [10] efforts, the first author's group focused on:

1. identifying where in the peptide (and into what kind of orbital and with what cross-section) the excess electron is *initially* bound,
2. characterizing to where, over what distances, and at what rates the electron may subsequently migrate within the peptide, and

* Corresponding author. Tel.: +1 8015818023.

E-mail address: simons@chem.utah.edu (J. Simons).

3. understanding how the excess electron's presence causes specific bonds (e.g., disulfide and backbone N–C_α bonds are found to preferentially break) to be cleaved and with what intensities.

As a result of our earlier studies and many more from the Turecek and other groups [11–39] and following early mechanistic proposals from the McLafferty and Zubarev groups [6–9], a picture has evolved within which it is the arrival of an electron at an amide π* or disulfide σ* orbital that causes the N–C_α or SS bond cleavage, respectively. The amide π* or disulfide σ* orbitals that are amenable to electron attachment are determined by the local intramolecular electrostatic potentials stabilizing the orbitals (if the potential is not sufficiently stabilizing, electron attachment cannot occur). Both Coulombic potentials from charged sites and dipole potentials [40–42] within the peptide have been suggested to play important roles both in guiding the ECD electron or ETD donor anion and in rendering the amide π* or disulfide σ* orbitals capable of accepting an electron.

In addition to contributing to the electrostatic potential within the peptide, the positive sites within the charged peptide provide Rydberg orbitals that act as “antennas” to which the electron is initially attached (either directly in ECD or via transfer from the anion donor in ETD), and subsequently serve to transfer the electron to amenable amide π* or disulfide σ* orbitals over distances determined by the radial sizes of the Rydberg orbitals.

The resulting mechanistic picture describes the ECD or ETD process as follows:

1. In both ECD and ETD, the electron most likely first attaches to a Rydberg orbital localized on a positively charged site (e.g., a protonated side chain or the protonated N-terminus) of the parent peptide as shown in Scheme 1. This positively charged site is often internally “solvated” via hydrogen bonding to, for example, a nearby carbonyl oxygen atom.
2. Within a Landau–Zener model, the initial electron attachment occurs at electron–peptide or anion donor–peptide distances that depend on the electron binding energy of the anion donor¹ and of the Rydberg orbital into which the electron is transferred.
3. Estimates of the electron attachment cross-sections based on such a model suggest that the accessible Rydberg principal quantum numbers (*n*) are limited to *n* = 3 and 4 in ETD¹ and *n* = 3–6 in ECD, and that each of these Rydberg levels is approximately equally populated.
4. After an excess electron is captured into a Rydberg orbital, it can subsequently undergo prompt (i.e., faster than relaxation within the Rydberg orbital manifold) intramolecular electron transfer to any SS σ* or amide π* orbital that lies within the radial shell of that Rydberg orbital but only if the the electron binding energy of that Rydberg orbital can be overcome by that of the SS σ* or amide π* orbital. This electron transfer step can be especially facile if the positively charged site on which the Rydberg orbital sits is hydrogen bonded to a nearby carbonyl oxygen atom as suggested in the pathway² labeled C in Scheme 1. However, as suggested by the pathway labeled UW in Scheme 1, it is also possible for the electron to transfer to more-distant SS σ* or amide π* orbitals, especially if the electron occupies a Rydberg orbital of large radial extent.
5. Once the electron enters an SS σ* orbital, cleavage of the associated disulfide bond is prompt because the σ²σ*¹ anionic

electronic state is repulsive. If the electron enters an amide π* orbital, cleavage of the N–C_α bond can occur by surmounting a thermally accessible barrier that is much smaller than the barrier needed to homolytically cleave this N–C_α bond in the absence of the excess electron.

6. After the electron attaches to an amide π* orbital, the N–C_α bond is weakened because cleaving it allows a new C=N π bond to form; this is why the barrier to cleavage is reduced. The [−]O=C=NH anion site can³ abstract a proton to form either the enolimine or the more stable amide. The proton is most likely abstracted from a proximal site of low proton binding strength. In either case, a closed-shell c fragment and an open-shell radical fragment are the result of the N–C_α cleavage.

In the present paper, we explore the implications of this model's prediction that *n* = 3 and 4 Rydberg orbitals will be equally populated in ETD and *n* = 3–6 Rydberg orbitals will be equally populated in ECD. In particular, we discuss what spatial distribution in the fragment-ion abundance patterns would be expected if these predictions are true, and we examine abundance patterns found in data obtained in experiments carried out under infrared photo-activation conditions where the parent-ion secondary structure is expected to be appreciably disrupted.

2. Theoretical analysis

Rydberg orbital manifolds occur at each positively charged site within a multiply charged polypeptide. Each Rydberg orbital can be characterized by a principal quantum number *n* that relates (approximately) to its electron binding energy as follows:

$$BE_{\text{Rydberg}}(n) \approx 13.6 \text{ eV}/n^2 \quad (1)$$

and to its radial “size” (i.e., the average value $\langle r \rangle$ of the distance of the electron from the center of positive charge) as

$$\langle r \rangle \approx 0.529 n^2 \text{ \AA} \quad (2)$$

In atomic cations, each Rydberg level having a given principal quantum number *n* has a family of orbitals characterized by orbital angular momentum quantum numbers *L* and *m*, with *L* running from 0 to *n* – 1. For molecular ions, the orbitals corresponding to this manifold of *n* different *L*-values and 2*L* + 1 different *m*-values still exist (i.e., one finds Rydberg orbitals having clear s, p, d, etc. angular nodal patterns), but their energy degeneracies are split by the local potential of the site at which the Rydberg orbitals are bound. Examples of several Rydberg orbitals of NH₄⁺, of ⁺NH₃–CH₃, and of (AR + 2H)²⁺ are shown in Fig. 1.

In addition to their low electron binding energies, which are even smaller than the valence electron binding energies of alkali cations, Rydberg orbitals are characterized by large radial extents (e.g., a 6s orbital has its highest density near 30 Å).

To achieve a more accurate description than provided by Eq. (1) for molecular Rydberg orbitals, it is common to characterize the electron binding energy in terms of a so-called quantum defect δ and a principal quantum number *n*

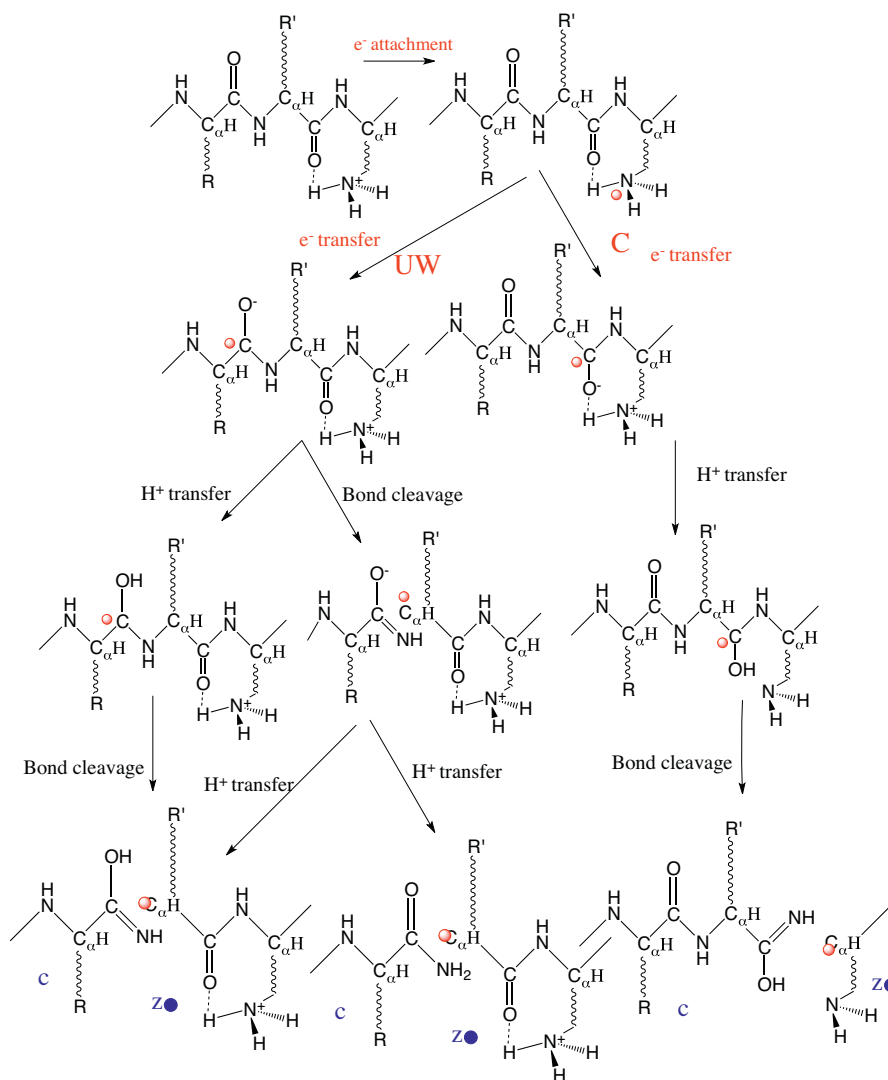
$$BE_{\text{Rydberg}}(n) \approx 13.6 \text{ eV}/(n - \delta)^2 \quad (3)$$

The quantum defect is introduced to (approximately) account for the fact that the Rydberg orbital is not fully screened from the

¹ In this paper, we assume a value for the electron binding energy BE_{Donor} of 0.6 eV (i.e., that of the commonly used fluoranthene anion) to characterize ETD, and a value of 0.0 eV is used to characterize the free electron used in ECD.

² This step can alternatively be viewed as involving transfer of a hydrogen atom from the hypervalent –NH₃ radical to the nearby carbonyl oxygen atom.

³ It is possible that the proton is abstracted prior to cleavage of the N–C_α bond, in which case formation of the enolimine would be favored. Some experimental infrared spectroscopic evidence exists [34] providing evidence that the amide is formed, but this is not conclusive support proving that the proton is transferred after N–C_α bond cleavage because the enolimine, if formed first, could subsequently rearrange to the thermodynamically more stable amide.



Scheme 1.

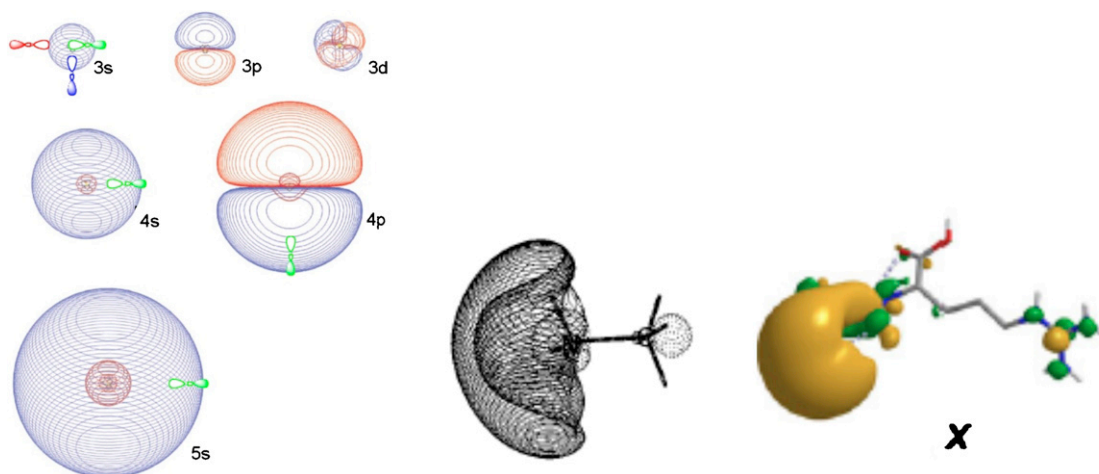


Fig. 1. 3s, 3p, 3d, 4s, 4p, and 5s Rydberg orbitals of NH_4^+ (left); the lowest (3s) Rydberg orbital of $^+\text{NH}_3\text{—CH}_3$ (middle); and the lowest Rydberg orbital of the dipeptide $(\text{AR} + 2\text{H})^{2+}$ (right). The latter figure is taken from Fig. 3 in Ref. [43].

underlying nuclear charges by the inner-shell orbitals. For example, in NH_4^+ , we view the lowest Rydberg state as having $n=3$ because nitrogen's 7 and the four protons' 4 positive charges are partially screened by the 10 total ($1s^2$ and $4s^2$) inner-shell electrons. That is, NH_4^+ is similar to Na^+ whose lowest unoccupied orbital is its 3s orbital. The energy needed to remove an electron from the 3s orbital of Na is 5.1 eV. To obtain this binding energy from Eq. (3) for $n=3$ would require a quantum defect of 1.37. The binding energy of the lowest Rydberg orbital of NH_4 is ca. 4 eV, which is not close to the estimate $13.6/3^2 = 1.5$ eV obtained from the hydrogenic expression of Eq. (1). However, if we take δ to be 1.16, Eq. (3) gives the correct 4 eV electron binding energy for the lowest $n=3$ state of NH_4 . This same quantum defect of 1.16 then predicts binding energies of 1.7, 0.9, and 0.6 eV for the $n=4$ –6 levels of NH_4 , respectively.

Because the radial extent of Rydberg orbitals also varies with n (see Eq. (2)), introduction of the quantum defect also alters estimates of these orbitals' sizes. Again using $\delta = 1.16$ to characterize NH_4^+ , we find ratios in the radial sizes of $n=3$ –6 Rydberg orbitals of $(n-\delta)^2/n^2 = 0.4, 0.5, 0.6,$ and 0.6 , compared to the size estimates obtained from the purely hydrogenic Eq. (2). That is, partial screening by inner-shell electrons radially contracts the $n=3$ –6 Rydberg orbitals by 40–60%. In the discussion given below, we use a factor of 50% to be representative of the average radial-scaling appropriate to the range of $n=3$ –6 Rydberg orbitals.

In the top portion of Fig. 2 we show the radial probability densities $r^2 \int \sin \theta \psi^*(r, \theta, \varphi) \psi(r, \theta, \varphi) d\theta d\varphi$ for hydrogen (i.e., assuming $\delta=0$) 3s, 4s, 5s, and 6s orbitals. Plots of Rydberg orbital densities appropriate to NH_4^+ (and, we believe, reasonably appropriate for protonated amine sites) would have their radial extents contracted by ca. 50% as explained above.

Notice that each Rydberg orbital has an outermost major radial peak and a series of minor peaks at smaller distances, that the location (r) and width T of the Rydberg orbitals' major radial peaks increases as n increases, and that the height of these major peaks decreases with n (e.g., $n=3$ is more strongly peaked near 7 Å than is $n=5$ near 14 Å). Orbitals with non-zero angular momentum have fewer radial nodes and are a bit more radially contracted than their corresponding s-orbitals described in Fig. 2. Moreover, as discussed earlier, limited screening as embodied by a non-zero quantum defect, causes the Rydberg orbitals of, for example, NH_4 , to be radially contracted relative to what is shown in Fig. 2. However, at all levels of theory, Rydberg orbitals are radially large, have small electron binding energies, and have major peaks whose width increases with n and whose height decreases with n . These attributes of Rydberg orbitals will be seen to be of much importance when predicting the spatial distribution of abundances of bond-cleavage fragment ions.

As noted earlier, our earlier mechanistic studies concluded that

1. $n=3$ and 4 Rydberg orbitals for ETD and $n=3$ –6 orbitals for ECD are approximately equally populated in the initial electron attachment event, and
2. the rate of electron transfer from such a Rydberg orbital to any SS σ^* or amide π^* orbital lying within that Rydberg orbital's major radial peak is fast compared to rates of relaxation among the Rydberg orbital manifold.

This is why we display radial electron densities for ensembles with (i) equal populations of $n=3$ and 4 Rydberg orbitals (for ETD) or with (ii) equal populations of $n=3$ –6 Rydberg orbitals (for ECD) in the bottom of Fig. 2.

The range of residues covered by the $n=3, 4$ and $n=5, 6$ Rydberg densities shown in the bottom part of Fig. 2 derive from assuming (i) a spacing of ca. 3 Å between neighboring backbone amide groups, (ii) a contraction of ca. 50% in the orbitals' radial extent when a quantum defect of 1.16 is used as discussed earlier, and (iii) that

the charged side chain's flexibility allows it to hydrogen bond to its nearest carbonyl site thus making the location of the positive site close to the side chain's neighbor's carbonyl oxygen. It is this assumption of internal solvation of the charged site that allows us to estimate the location of the Rydberg-bound electron relative to the backbone amide sites independent of the length of the side chain possessing the charged site.

The 3 Å inter-residue distance may be appropriate for a spatially extended polypeptide, but not if the peptide is highly folded or globular. Moreover, each of the positive sites within a peptide sample used in ECD or ETD adopts a dynamically changing range of positions (e.g., the basic side chains and even the N-terminus are flexible) and the electron density experienced by any given SS σ^* or amide π^* orbital will depend on its instantaneous distance from the positive site holding the attached electron. For these reasons, it is best to average the density plots in Fig. 2 over a range of distances characterizing the location of the charge site holding the electron. With these caveats in mind, we think it still reasonable that these plots predict high cleavage rates between 1 and 5 residues from positive sites whose $n=3, 4$ Rydberg orbitals are populated and lower cleavage rates beyond the 5th residue out to ca. 9 residues in ECD where the $n=5, 6$ orbitals are also populated.

In summary, we expect certain major features contained in the idealized data of Fig. 2 (with radial distances scaled to reflect the quantum defect) to persist in real Rydberg orbital densities:

1. The $n=3, 4$ density has high amplitude between residues 1 and 5.
2. The $n=5, 6$ density (i.e., the difference between the red and yellow plots in the bottom of Fig. 2), which we suggest accounts for density present in ECD but not in ETD, arises mainly between residues 4 and 9.
3. The intensity of the $n=3, 4$ density is higher within its primary range than is the $n=5, 6$ density within its primary range.

With this picture of the $n=3, 4$ and $n=3$ –6 electron densities in mind, we now put forth the main predictions of this paper.

1. In ETD,¹ the abundance of c or z* fragments resulting from N–C α cleavage should reflect that spatial distribution of $n=3$ and $n=4$ Rydberg orbitals around each charged site, and
2. In ECD, the abundance of c or z* fragments resulting from N–C α cleavage should reflect that spatial distribution of $n=3$ through $n=6$ Rydberg orbitals around each charged site, with higher abundance in the range of the $n=3, 4$ Rydberg orbitals.
3. Because electron attachment to various charged sites need not occur with equal probability, the total abundances associated with these sites can differ.

Because the $n=3, 4$ distribution has higher intensity for r -values falling within its major peak than does the $n=5, 6$ distribution within its major peak, we predict more bond cleavage 1–5 residues from a positive site holding the attached electron and, for ECD but not ETD, relatively less cleavage 6–9 residues from this site. Moreover, for reasons explained earlier, we do not expect the cleavage patterns to display the fine details (e.g., nodes and oscillations) shown in Fig. 2.

The predictions just put forth do not take into consideration the nature of the spatial distribution of amino acid side chains within the peptide. They focus only on the $n=3, 4$ or $n=3$ –6 Rydberg densities' spatial extent as a measure of the potential of these densities to deliver the attached electron to various amide π^* orbitals. As we will see later, the physical characters of the side chains can indeed alter the product ion abundance patterns beyond what the current model suggests. Within our model, this means that the ability of a particular amide π^* orbital to accept the attached electron from a

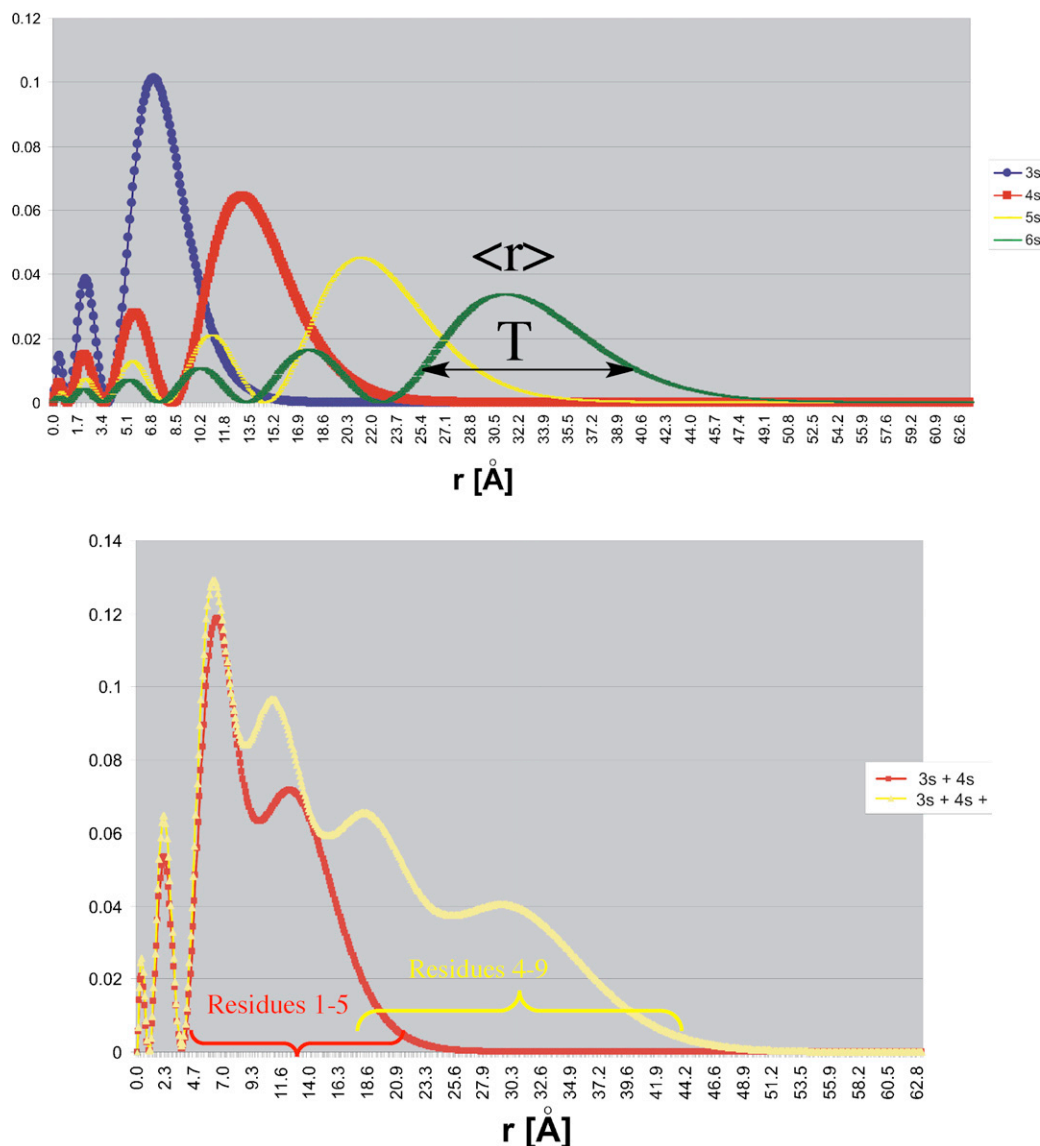


Fig. 2. Radial probability densities (in units of \AA^{-1}) for 3s, 4s, 5s, and 6s Rydberg orbitals (top), and (bottom) radial densities for ensembles containing equal populations of $n=3$ and 4 Rydberg orbitals (red) and equal populations of $n=3$ –6 Rydberg orbitals (yellow). Also shown are the ranges of residues these two densities primarily cover along an extended backbone, taking into account the shrinkage in radial distances associated with a quantum defect of 1.16 (see text for details).

Rydberg orbital depends on the nature of the side chain attached to that amide's α carbon atom. Other studies [44–47] have examined how various physical properties of the side chains can alter the cleavage rates of nearby N–C $_{\alpha}$ bonds and have even made use of these effects by introducing artificial (predator) side chains [48] that capture ETD or ECD electrons thus interrupting the usual N–C $_{\alpha}$ bond cleavages.

In the following section, we examine selected experimental data to ascertain whether the abundances of c or z $^{\bullet}$ fragments do or do not agree with the predictions about the range (e.g., 1–5 residues for ETD) and spatial distribution (e.g., peaking around residues 1–3 for ETD) of fragment ions around each positive site. We focus on experiments in which infrared photo-activation steps are taken in conjunction with the ETD or ECD as a means for disrupting the secondary structure (i.e., folding, internal solvation, and hydrogen bonding) of the parent ion. This is done because we believe it is under such conditions that we can reasonably estimate the distances between the sites holding the Rydberg electron and the backbone amide sites. As will be seen, the spatial distribution of fragment ions that we are considering tells only part of the story,

and the nature of the side chains as well as residual parent-ion structure that remains, even when infrared activation techniques have been employed, are part of the full story.

3. Analysis of experimental data

In Fig. 3 we display experimental data [49] taken from the Coon laboratory at Madison, Wisconsin, where the second author is actively involved. At the top of the figure, data obtained by first carrying out ETD (using azulene, which has an electron binding energy of 0.8 eV, close to the 0.6 eV value assumed in this paper, as the donor anion [50]) and subsequently submitting the non-dissociated electron transfer species to gentle resonant-excitation collisionally activated dissociation (the combined process termed ETcAD [51]). At the bottom of the figure, we see data on the same system obtained by simultaneously subjecting the parent-ion sample to infrared photons and to azulene anions, thus achieving so-called activated-ion ETD (AI-ETD). As explained in Ref. [49], the infrared activation is assumed to heat the parent ions sufficiently to disrupt secondary structure, thus (presumably) rendering the ensemble of

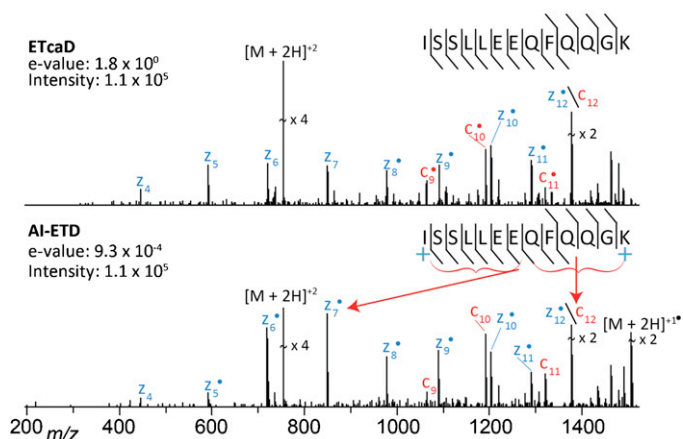


Fig. 3. ETcAD and AI-ETD spectra of doubly charged ISSLLEEQFQQGK taken from Fig. 4 of Ref. [43]. The positive sites are labeled with blue + signs, and the 1–5 residue ranges of the $n = 3, 4$ Rydberg densities on the N-terminus and the K sites are shown as red brackets. For AI-ETD, a laser power of ~ 40 W was utilized; for ETcAD, the supplemental CAD excitation utilized an excitation voltage of ~ 1 V and a q -value of ~ 0.18 for the charge-reduced precursor. (For interpretation of the references to color in this figure legend, the reader is referred to the web version of the article.)

ions that subsequently undergo ETD fragmentation more spatially extended than in the original sample. Of course, the average gas phase conformation of precursor peptides is not expected to rigidly linear; however, based on observations related to the degree of H-atom transfers between newly formed c/z ion pairs noted among ETD, AI-ETD, and ETcAD spectra in Ref. [49], it is our expectation that data on extended structures are more likely to follow the predictions we made earlier because, for such structures, the distances from charged sites to backbone amide units can be estimated with reasonable confidence.

ETcAD spectra typically comprise a mixture of odd and even electron product ions for both c - and z -type product ions. While ETD typically results in the exclusive production of c - and z^* -ions, ETcAD also produces c^* and z -ions, nominally shifted ~ 1 Da from their predicted mass. It is believed that these shifted ions arise via an H-atom transfer occurring between c - and z -ions that are bound together immediately following dissociation [52,53] (note that such H-atom transfers have been found to take place on an extremely rapid timescale [54]). For all ETcAD data shown herein, the supplemental excitation voltage was approximately equal to 1 V, with a q -value of ~ 0.18 for the charge-reduced precursor (ETnoD species).

In contrast, spectra arising from AI-ETD data are dominated by c/z^* fragments, which we believe indicates that fragmentation occurred promptly after $N-C_\alpha$ bond cleavage. Assuming that the infrared excitation indeed disrupts much of the peptide secondary structure, such data should give us the best chance for testing the predictions made earlier in this paper. For all AI-ETD data shown, photon wavelength was $\sim 10.6 \mu\text{m}$, with a photon flux of 40–50 W unless otherwise indicated.

There clearly are significant differences between the ETcAD and AI-ETD data even if we focus on the c/z^* fragment ions that are presumed to result from prompt cleavage of $N-C_\alpha$ bonds. To a reasonable extent, the AI-ETD abundances appear to be in line with what our model predicts:

- i. 1–5 residues from the K site, fragments c_{12} , c_{11} , c_{10} , $c_9 + z_4^*$, and z_5^* comprise one spatial distribution;
- ii. 1–5 residues from the N-terminus, fragments z_{12}^* , z_{11}^* , z_{10}^* , z_9^* , and z_8^* form another,

both of which have low abundance one residue displaced from the respective charged site, a maximum in abundance one or two

residues more distant, and then decreasing abundance (except for z_6^* and z_7^* , which we discuss below).

Before discussing the two features that do not fit our expectations, let us reflect on what the data in Fig. 3 might suggest about when proton transfer is taking place relative to when $N-C_\alpha$ bond cleavage occurs. First, we note that the AI-ETD spectrum shows far more z^* than c fragment ions. Likely, this is because formation of c ions requires a proton to transfer from the less acidic protonated K residue than the more acidic protonated N-terminus. To form the closed-shell c_{12} through c_9 ions within the mechanism in Scheme 1, a proton must be transferred from the C-terminal direction, presumably from the protonated Lys. To form the open-shell z_5^* ion, proton transfer from the Lys must not be taking place (otherwise, c_8 would form). So, it appears that proton transfer from the Lys site is limited to distances corresponding to ca. 4 residues. However, two of the most abundant ions in Fig. 3 are z_6^* and z_7^* , which lie 7 and 6 residues from the protonated N-terminus and 6 and 7 residues from the Lys, respectively. Although not conclusive, these observations seem to be most consistent with a view in which the proton transfer takes place after cleavage of the $N-C_\alpha$ bond. For z_6^* or z_7^* to be formed with proton transfer taking place prior to bond cleavage would require either the Lys or the protonated N-terminus to transfer its proton over 6 or 7 residues, which one would expect to be less likely than transfer over fewer residues and which seems inconsistent with the high abundances of z_6^* and z_7^* .

As noted earlier, a feature of the abundance pattern in Fig. 3 that does not seem to fit in with our predictions is the high intensities of the c_{12} and z_{12}^* fragments. These enhanced intensities suggest that both the protonated N-terminus and the C-terminal charged K are internally solvated to proximal amide carbonyl groups and thus may generate cleavage of the $N-C_\alpha$ bonds closest to them as the pathway labeled C in Scheme 1 describes. In such a case, attachment of an electron into an $n = 3$ Rydberg orbital at either of these sites could, via this Cornell-like mechanism [6] (which is why we used the label C in Scheme 1) generate facile cleavage to generate the observed c_{12} and z_{12}^* fragments. It would have to be an $n = 3$ Rydberg orbital because this orbital has the correct radial size and thickness to connect the protonated amine and the solvated amide π^* orbital and because it is known [55] that this $n = 3$ state undergoes facile H atom loss, whereas the states with $n > 3$ do not.

In summary, it may well be that cleavage of $N-C_\alpha$ bonds within amide units not intimately involved in internal solvation occurs via the pathway labeled UW in Scheme 1 while cleavage of $N-C_\alpha$ bonds whose amide carbonyls are involved in internal solvation follows the pathway labeled C in Scheme 1. It makes sense that the efficiency of $N-C_\alpha$ bond cleavage when internal solvation is present should be especially high because of the small distance between the charged site (from which the proton can also come) and the amide unit. Moreover, we note that internal solvation of charged Lys (either to the C-terminal COOH group or to a carbonyl unit in the opposite direction) and of the protonated N-terminus (to a nearby carbonyl) are commonly encountered.

One might be tempted to suggest that all of the $N-C_\alpha$ bond cleavages occur along the C pathway. However, this would require that the protonated N-terminus or K be involved in solvation events with amide carbonyl groups over 6 residues and to occur with a population that mimics the product ion abundance pattern seen in Fig. 3. It is difficult to imagine why a solvation pattern like this would occur, so we believe this proposal is unlikely true.

So, if formation of c_{12} and z_{12}^* is dominated by the Cornell pathway and the UW pathway of Scheme 1 (with the associated spatial distribution of the $n = 3, 4$ Rydberg densities) accounts for c_{12} , c_{11} , c_{10} , $c_9 + z_4^*$, and z_5^* as well z_{12}^* , z_{11}^* , z_{10}^* , z_9^* , and z_8^* , why are the intensities of z_6^* and z_7^* so high? One possibility is the presence of the acidic Glu side chains on the amides giving rise to these fragments. The Tsybin group has found [56] enhancements in product

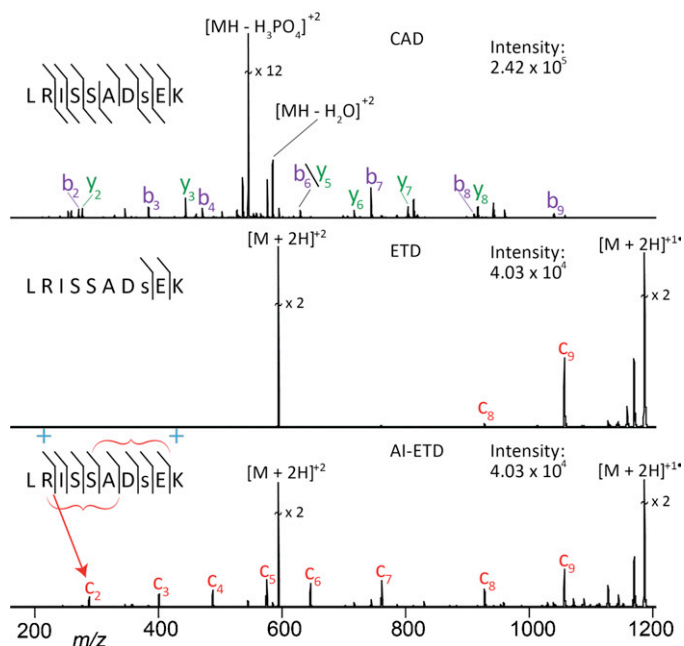


Fig. 4. CAD, ETD, and AI-ETD spectra of doubly protonated LRISSADsEK taken from Fig. 5 of Ref. [49]. The positive sites are labeled with blue + signs, and the 1–5 residue ranges of the $n = 3, 4$ Rydberg densities on the R and K sites are shown as red brackets. The lower case 's' denotes a phosphorylated serine residue. For AI-ETD, a laser power of ~ 30 W was used. (For interpretation of the references to color in this figure legend, the reader is referred to the web version of the article.)

ion abundances near such side chains in studies of doubly charged H-Arg(Gly)₄-X-(Gly)₄Lys-OH and of H-Arg(Ala)₄-X-(Ala)₄Lys-OH, when X, which labels an amino acid that varies in the experiment, has an acidic side chain. The abundances of the z_6^* and z_7^* ions suggest that side chain properties likely do affect the rates of production of various fragment ions. Those studies were focused on identifying differences in bond cleavage rates associated with various physical properties (e.g., basicity, hydrophobicity, polarity) of the amino acids' side chains. In the present study, we are ignoring such differences and emphasizing the spatial distribution of the $n = 3, 4$ (for ETD) and $n = 3-6$ (for ECD) Rydberg orbitals as a contributor to the distribution of bond cleavages and hence of fragment abundances. The observation of enhanced intensities in the z_6^* and z_7^* ions suggest that side chain identity also needs to be taken into consideration.

In Fig. 4, we see another set of data from the Coon lab in which ETD, AI-ETD and resonant-excitation collision-activated dissociation (CAD) data were obtained. As expected, the CAD data differ tremendously from either the ETD or AI-ETD data and display a fragmentation pattern more typical of collisional dissociation.

The main difference between the ETD and AI-ETD data is the appearance of far more fragment ions in the latter, with fragments derived from N-C_α bond cleavages extending five residues from the charged R and K sites. Although the fragment ion intensities do not differ as greatly as in Fig. 3, it seems that higher abundance occurs in the c_5 to c_7 range (i.e., 3–5 residues from either of the charged sites) with the abundance pattern similar to the $n = 3, 4$ Rydberg orbital density ranging from c_2 through c_8 . The fact that only c ions are observed is likely a result of proton transfer taking place from the more acidic protonated K than from the less acidic protonated R. The fact that proton transfer is taking place and, for c_2 specifically, from 7 residues away from R again suggests that this transfer takes place after N-C_α bond cleavage rather than before.

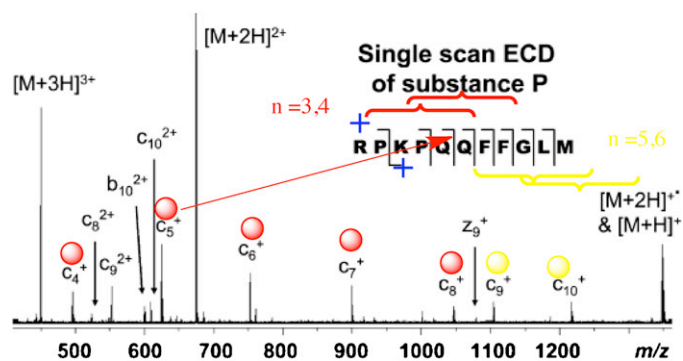


Fig. 5. ECD data generated using triply-protonated substance P: RPKPKQFFGLM with the two positive sites of the doubly charged ion labeled in blue and the ranges of the $n = 3, 4$ and $n = 5, 6$ Rydberg densities shown with red and yellow brackets, respectively. Data taken from Fig. 3 in Ref. [57]. (For interpretation of the references to color in this figure legend, the reader is referred to the web version of the article.)

The somewhat enhanced c_9 abundance could be due to electron attachment to the internally solvated protonated K terminus generating enhanced cleavage via a Cornell-type mechanism as discussed earlier. The fact that c_2 is not correspondingly enhanced would be consistent with the protonated R, even if solvated to the proximal amide carbonyl, not being able to take part in the Cornell mechanism. Indeed, in Ref. [16], evidence is discussed that supports this view; the fact that R is considerably more basic than K or than the N-terminal amine causes the protonated R's ground Rydberg state to have a substantial energy barrier for transferring an H atom to solvation-partner carbonyl oxygen.

In Fig. 5, we display data on substance P collected by Tsybin et al. [57] using ECD methods with simultaneous infrared excitation [58,59], the latter being utilized for reasons similar to the use of IR radiation in AI-ETD- to disrupt secondary structure.

In this data, we see a pattern of c ions (c_4 through c_8 with a peak at c_5) that is consistent with the shapes of the $n = 3, 4$ distributions surrounding the R or K sites. The c_9 and c_{10} ions could come from the $n = 5, 6$ distribution or from the tail end of the $n = 3, 4$ distribution if dynamical motion of the C-terminus of the peptide (see the next paragraphs for more detail) caused these residue to approach the R or K site. The fact that primarily c rather than z^* ions are observed is not surprising in this case (to form z^* ions would require transfer of a proton from the positively charged c residue to the neutral z^* fragment) and sheds no light on the issue of when and if proton transfer is taking place. Moreover, the lack of enhancement in cleavages proximal to but in the C-terminal direction from R or K (i.e., enhancement due to involvement of a Cornell mechanism) is also not surprising because the neighboring Pro groups block backbone cleavage at these sites.

Next, in the bottom part of Fig. 6, we display ECD fragment ion data from Tsybin and co-workers for a doubly charged REYPLLR fragment ion obtained by first subjecting doubly charged SDREYL-LIR to infrared multi-photon dissociation.

Again, we see a distribution of N-C_α cleavage products (c_4 through c_7) that seems to mimic the spatial distribution of the $n = 3, 4$ Rydberg orbitals on the two charged R sites. No c_3 ions can be formed because of the Pro residue. Moreover, the lack of enhancement in the c_7 abundance suggests that the C-terminal protonated R is not capable of participating in the Cornell type mechanism probably for reasons we explained earlier. Finally, the fact that c ions rather than z^* ions are observed means that proton transfer from the C-terminal protonated R site must be taking place (and over up to 4 residues).

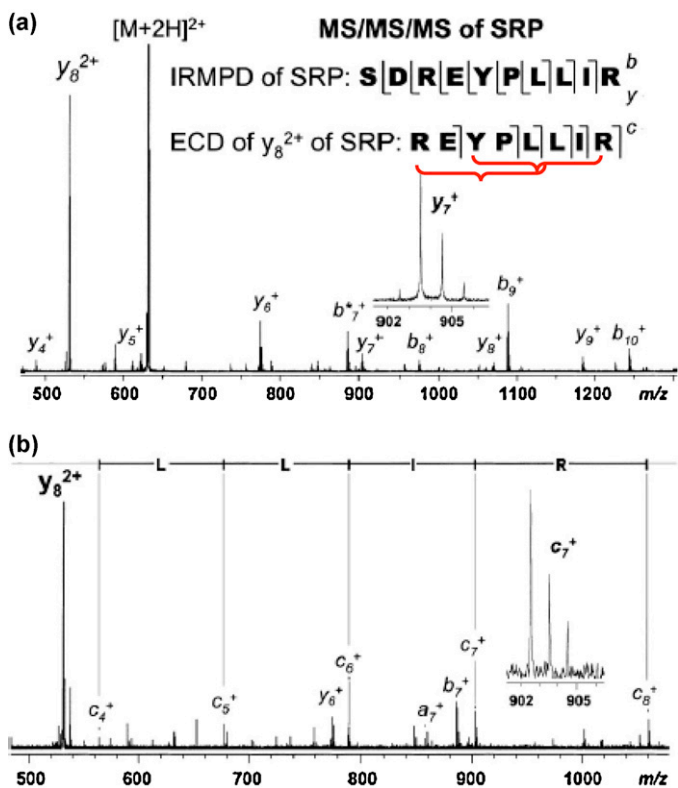


Fig. 6. ECD data on doubly charged REYPLLIIR (bottom). Taken from Fig. 6 in Ref. [57]. The ranges of the $n=3, 4$ Rydberg orbitals' densities on the two charged R sites are shown with red brackets. (For interpretation of the references to color in this figure legend, the reader is referred to the web version of the article.)

In Fig. 7, we see another set of AI-ETD data from the Coon laboratory on the doubly charged DNIQGITKPAIR.

The abundance pattern for z_6^+ through z_{11}^+ seems to fit the $n=3, 4$ density profile for Rydberg orbitals centered on the K site. The somewhat enhanced intensity of z_5^+ could arise via a Cornell-type mechanism resulting from the protonated K site being solvated to a nearby carbonyl oxygen. For reasons explained earlier, it is unlikely that c_{11} could arise from analogous solvation of the charged R site in a Cornell-like mechanism.

Let us finish with an example that could be used to further test the ideas about fragment ion abundance patterns put forth here.

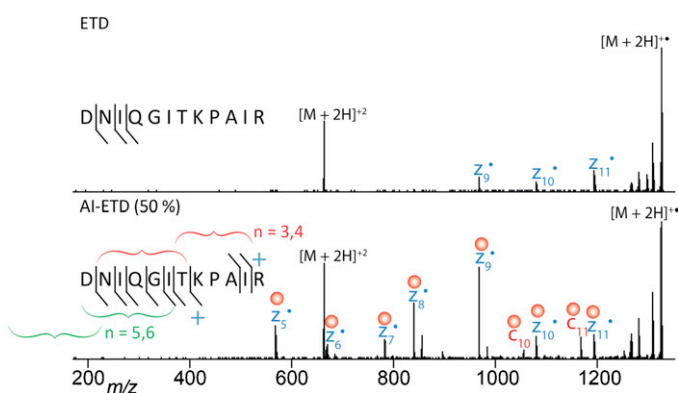


Fig. 7. ETD and AI-ETD resulting from MS/MS interrogation of doubly protonated DNIQGITKPAIR. The ranges of the $n=3, 4$ Rydberg orbitals' densities on the charged R and K sites are shown with red brackets. For AI-ETD, a laser power of 40W was used. (For interpretation of the references to color in this figure legend, the reader is referred to the web version of the article.)



Fig. 8. Structure of doubly charged $(AcCA_jK+H)_2^{2+}$ (for $j=15$) showing the central disulfide linkage, two α -helices, two C-terminal protonated Lys residues, and the four $N-C_\alpha$ bonds that are cleaved under ECD conditions. Also shown as red brackets are the ranges of the $n=3, 4$ Rydberg densities at the two Lys sites. (For interpretation of the references to color in this figure legend, the reader is referred to the web version of the article.)

In Fig. 8, we display a representation of the structure of doubly charged peptides $(AcCA_jK+H)_2^{2+}$ that were studied using ECD in the Marshall laboratory (A. Marshall, K. Håkansson, personal communication to J.S.).

In those ECD experiments, abundant fragment ions arising from cleaving the SS bond were found (for $j=10, 15$, and 30 where the distances from the terminal Lys to the SS bond were estimated to be ca. 18, 24, and 32 Å, respectively). Moreover, substantial $N-C_\alpha$ cleavage at the four C-terminal Ala sites was also observed. Using an estimate that each turn of the α -helix is ca. 1.5 Å in length (whereas the spacing between amide linkages in an extended backbone is ca. 3 Å), this suggests that the fourth $N-C_\alpha$ cleavage occurs up to ca. 6 Å from the Lys.

As discussed in detail in Ref. [42], the Marshall group's findings on $(AcCA_jK+H)_2^{2+}$ are fully in line with the ideas developed in our earlier work. In particular, we note that

1. The Coulomb and dipole stabilizations of the protonated Lys residues and of the two oppositely directed Ala α -helices, respectively, cause electron attachment to the SS σ^* orbital to be 4 eV exothermic for the $j=15$ species. Although a bit less so for the $j=20$ peptide, it is still more than enough to allow the SS σ^* orbital to extract an electron from an $n=5$ or $n=6$ Rydberg orbital on either Lys site. Moreover, as seen in Fig. 2, the distance between either Lys and the SS bond lies within the radial extent of the $n=5, 6$ Rydberg orbitals' density but not within that of the $n=3, 4$ density. As a result, it makes sense that disulfide cleavage is observed for $j=10, 15$, or 20 under ECD conditions where the $n=5, 6$ density is operative.
2. The electrostatic stabilization near any of the four C-terminal amide groups exceeds 2 eV, as a result of which electron attachment to any of their π^* orbitals is exothermic. The distance between the Lys and any of these four amide units falls within the $n=3, 4$ Rydberg orbital density. So, it is also reasonable that cleavage of the four C-terminal $N-C_\alpha$ bonds is observed under ECD. It is also reasonable that a Cornell-type mechanism could be operative in cleaving some of the C-terminal $N-C_\alpha$ bonds since the protonated Lys sites are, as shown in Fig. 8, involved in hydrogen bonds to nearby carbonyl oxygen atoms.

However, the model put forth in this paper predicts that, under ETD conditions, where the $n=5, 6$ Rydberg orbital density is not operative, cleavage of the disulfide bond should not be observed although cleavage at the four C-terminal $N-C_\alpha$ bonds should still be found. Thus, a good test of our predictions would involve carrying out ETD experiments on species like that shown in Fig. 8 using a donor anion that can populate $n=3, 4$ Rydberg orbitals, but not $n=5, 6$ orbitals.

Another interesting feature of the ECD data reported in A. Marshall, K. Håkansson (personal communication to J.S.) is that

N–C $_{\alpha}$ was limited to the four C-terminal residues. This is surprising because the radial extent of the $n = 3, 4$ Rydberg orbitals is larger than four residues, as evidenced by the data reported in Figs. 3–7, especially because the α -helices shorten distances between amide groups along the backbone. Therefore, it would be helpful to carry out an AI-ETD experiment on (AcCA $_n$ K+H) $_2^{2+}$ to see whether infrared activation could either disrupt some of the α -helix structure and expose more of the N–C $_{\alpha}$ bonds to cleavage.

4. Summary

Predictions from earlier work by the Simons group suggest that $n = 3–6$ Rydberg orbitals are populated in ECD and $n = 3, 4$ orbitals in ETD using anion donors having electron binding energies near 0.6 eV, and that the populations of these orbitals are approximately equal. Based on these predictions, in the present manuscript we postulate that the distribution of abundances in N–C $_{\alpha}$ bond cleavages along the backbone of a multiply charged parent peptide ion will mimic the spatial distribution of the $n = 3, 4$ (for ETD) or $n = 3–6$ (for ECD) Rydberg orbitals on the charged sites. These predictions are tested on a series of ECD and ETD data obtained under conditions (i.e., simultaneous infrared activation) that are believed to disrupt much of the parent ion's secondary structure thus rendering it maximally extended, which makes distance estimates based on location of various amide units along the backbone most reliable.

It is found that the fragment ion abundance patterns do mimic the spatial extents and general shapes of the Rydberg orbitals' densities, but with two additional features. First, there appears to be enhanced N–C $_{\alpha}$ bond cleavage immediately proximal to charged Lys or N-terminal amine sites; such enhancement is rationalized in terms of contributions from a so-called Cornell mechanism when these charged sites are internally solvated to a nearby amide carbonyl group. Secondly, there are a few variations within the general outline of the Rydberg orbitals' density patterns that we attribute to effects from the physical nature of the associated side chains. This effect seems to be most pronounced for acidic side chains.

References

- [1] J.E.P. Syka, J.J. Coon, M.J. Schroeder, J. Shabanowitz, D.F. Hunt, Proceedings of the National Academy of Sciences of the United States of America 101 (2004) 9528–9533.
- [2] J.J. Coon, J.E.P. Syka, J.C. Schwartz, J. Shabanowitz, D.F. Hunt, International Journal of Mass Spectrometry 236 (2004) 33–42.
- [3] S.J. Pitteri, P.A. Chrisman, S.A. McLuckey, Analytical Chemistry 77 (2005) 5662–5669.
- [4] H.P. Gunawardena, M. He, P.A. Chrisman, S.J. Pitteri, J.M. Hogan, B.D.M. Hodges, S.A. McLuckey, Journal of the American Chemical Society 127 (2005) 12627–12639.
- [5] H.P. Gunawardena, L. Gorenstein, D.E. Erickson, Y. Xia, S.A. McLuckey, International Journal of Mass Spectrometry 265 (2007) 130–138.
- [6] R.A. Zubarev, N.L. Kelleher, F.W. McLafferty, Journal of the American Chemical Society 120 (1998) 3265–3266.
- [7] R.A. Zubarev, N.A. Kruger, E.K. Fridriksson, M.A. Lewis, D.M. Horn, B.K. Carpenter, F.W. McLafferty, Journal of the American Chemical Society 121 (1999) 2857–2862.
- [8] R.A. Zubarev, D.M. Horn, E.K. Fridriksson, N.L. Kelleher, N.A. Kruger, M.A. Lewis, B.K. Carpenter, F.W. McLafferty, Analytical Chemistry 72 (2000) 563–573.
- [9] R.A. Zubarev, K.F. Haselmann, B. Budnik, F. Kjeldsen, R. Jensen, European Journal of Mass Spectrometry 8 (2002) 337–349.
- [10] A recent summary of our work appears in J. Simons, Journal of the American Chemical Society 132 (2010) 7074–7085.
- [11] E.A. Syrstad, F. Turecek, Journal of Physical Chemistry A 105 (2001) 11144–11155.
- [12] F. Turecek, E.A. Syrstad, Journal of the American Chemical Society 125 (2003) 3353–3369.
- [13] F. Turecek, M. Polasek, A. Frank, M. Sadilek, Journal of the American Chemical Society 122 (2000) 2361–2370.
- [14] E.A. Syrstad, D.D. Stephens, F. Turecek, Journal of Physical Chemistry A 107 (2003) 115–126.
- [15] F. Turecek, Journal of the American Chemical Society 125 (2003) 5954–5963.
- [16] E.A. Syrstad, F. Turecek, The American Society for Mass Spectrometry 16 (2005) 208–224.
- [17] E. Uggerud, International Journal of Mass Spectrometry 134 (2004) 45–50.
- [18] I. Anusiewicz, J. Berdys-Kochanska, J. Simons, Journal of Physical Chemistry A 109 (2005) 5801–5813.
- [19] I. Anusiewicz, J. Berdys-Kochanska, P. Skurski, J. Simons, Journal of Physical Chemistry A 110 (2006) 1261–1266.
- [20] A. Sawicka, P. Skurski, R.R. Hudgins, J. Simons, Journal of Physical Chemistry B 107 (2003) 13505–13511.
- [21] M. Sobczyk, P. Skurski, J. Simons, Advances in Quantum Chemistry 48 (2005) 239–251.
- [22] A. Sawicka, J. Berdys-Kochanska, P. Skurski, J. Simons, International Journal of Quantum Chemistry 102 (2005) 838–846.
- [23] I. Anusiewicz, J. Berdys, M. Sobczyk, A. Sawicka, P. Skurski, J. Simons, Journal of Physical Chemistry A 109 (2005) 250–258.
- [24] V. Bakken, T. Helgaker, E. Uggerud, European Journal of Mass Spectrometry 10 (2004) 625–638.
- [25] P. Skurski, M. Sobczyk, J. Jakowski, J. Simons, International Journal of Mass Spectrometry 265 (2007) 197–212.
- [26] M. Sobczyk, D. Neff, J. Simons, International Journal of Mass Spectrometry 269 (2008) 149–164.
- [27] M. Sobczyk, J. Simons, International Journal of Mass Spectrometry 253 (2006) 274–280.
- [28] M. Sobczyk, J. Simons, Journal of Physical Chemistry B 110 (2006) 7519–7527.
- [29] D. Neff, M. Sobczyk, J. Simons, International Journal of Mass Spectrometry 276 (2008) 91–101.
- [30] D. Neff, J. Simons, International Journal of Mass Spectrometry 277 (2008) 166–174.
- [31] F. Turecek, X. Chen, C. Hao, Journal of the American Chemical Society 130 (2008) 8818–8833.
- [32] X. Chen, F. Turecek, Journal of the American Chemical Society 128 (2006) 12520–12530.
- [33] A.J.S. Holm, M.K. Larsen, S. Panja, P. Hvelplund, S. Brøndsted Nielsen, R.D. Leib, W.A. Donald, E.R. Williams, C. Hao, F. Tureček, International Journal of Mass Spectrometry 276 (2008) 116–126.
- [34] J. Chamot-Rooke, C. Malosse, G. Frison, F. Tureček, Journal of the American Society for Mass Spectrometry 18 (2007) 2146–2161.
- [35] Y.M.E. Fung, T.-W.D. Chan, Journal of the American Society for Mass Spectrometry 16 (2005) 1523–1535.
- [36] H. Konishi, Y. Yokotake, T. Ishibahsia, Journal of the Mass Spectrometry Society of Japan 50 (2002) 229–232.
- [37] A.J.S. Holm, P. Hvelplund, U. Kadhane, M.K. Larsen, B. Liu, S.B. Nielsen, S. Panja, J.M. Pedersen, T. Skryudstrup, K. Stochkel, E.R. Williams, E.S. Worm, Journal of Physical Chemistry A 111 (2007) 9641–9643.
- [38] D. Neff, J. Simons, Journal of Physical Chemistry A 114 (2010) 1309–1323.
- [39] J. Simons, Chemical Physics Letters 484 (2010) 81–95.
- [40] C.L. Moss, T.W. Chung, J.A. Wyer, S. Brøndsted Nielsen, P. Hvelplund, F. Turecek, Journal of the American Society for Mass Spectrometry 22 (2011) 731–751.
- [41] Analogous "guiding" of ECD electrons was suggested even earlier in F. Turecek, T.W. Chung, C.L. Moss, J.A. Wyer, A. Ehlerding, H. Zettergren, S.B. Nielsen, P. Hvelplund, J. Chamot-Rooke, B. Bythell, B. Paizs, Journal of the American Chemical Society 132 (2010) 10728–10740.
- [42] I. Świercz, P. Skurski, J. Simons, Journal of Physical Chemistry A 116 (2012) 1828–1837.
- [43] C.L. Moss, W. Liang, X. Li, F. Tureček, Journal of the American Society for Mass Spectrometry 23 (2012) 446–459.
- [44] Z. Zhang, Analytical Chemistry 82 (2010) 1990–2006.
- [45] A. Vorobyev, H. Ben Hamidane, Y.O. Tsybin, Journal of the American Society for Mass Spectrometry 20 (2009) 2273–2283.
- [46] Y.O. Tsybin, K.F. Haselmann, M.R. Emmett, C.L. Hendrickson, A.G. Marshall, Journal of the American Society for Mass Spectrometry 17 (2006) 1704–1711.
- [47] H. Ben Hamidane, H. He, O.Yu. Tsybin, M.R. Emmett, C.L. Hendrickson, A.G. Marshall, Y.O. Tsybin, Journal of the American Society for Mass Spectrometry 20 (2009) 1182–1192.
- [48] C.H. Sohn, C.K. Chung, S. Yin, P. Ramachandran, J.A. Loo, J.L. Beauchamp, Journal of the American Chemical Society 131 (2009) 5444–5459.
- [49] A.R. Ledvina, N.A. Beauchene, G.C. McAlister, J.E.P. Syka, J.C. Schwartz, J. Griep-Raming, M.S. Westphall, J.J. Coon, Analytical Chemistry 82 (2010) 10068–10074.
- [50] As discussed in Ref. [10], the electron binding energy of the donor anion determines which Rydberg orbitals are predicted to be populated. For an electron binding energy of zero, representative of EDC, the $n = 3–6$ Rydberg orbitals are predicted to be populated. For an anion donor with an electron binding energy of 0.6 eV, only $n = 3$ and 4 are populated. So, for anions with binding energies much above 0.6 eV, one could limit the Rydberg states to only $n = 3$; alternatively by lowering the binding energy below 0.6 eV, one could populate $n = 5$ and even $n = 6$, for a very small binding energy.
- [51] D.L. Swaney, G.C. McAlister, M. Wirtala, J.C. Schwartz, J.E.P. Syka, J.J. Coon, Analytical Chemistry 79 (2007) 477–485.
- [52] P.B. O'Connor, C. Lin, J.J. Cournoyer, J.L. Pittman, M. Belyayev, B.A. Budnik, Journal of the American Society for Mass Spectrometry 17 (2006) 576–585.
- [53] M.M. Savitski, F. Kjeldsen, M.L. Nielsen, R.A. Zubarev, Journal of the American Society for Mass Spectrometry 18 (2007) 113–120.
- [54] C. Lin, J.J. Cournoyer, P.B. O'Connor, Journal of the American Society for Mass Spectrometry 19 (2008) 780–789.
- [55] This issue is illustrated nicely in Ref. [16].

- [56] See Ref. [46] as well as A. Vorobyev, H.B. Hamidane, P. Campomanes, S. Vanni, F. Chiro, U. Rothlisberger, Y.O. Tsybin, *Journal of the American Society for Mass Spectrometry*, in press.
- [57] Y.O. Tsybin, M. Witt, G. Baykut, F. Kjeldsen, P. Håkansson, *Rapid Communications in Mass Spectrometry* 17 (2003) 1759–1768.
- [58] Earlier, the McLafferty group showed that collisional activation carried out simultaneously with ECD could also serve to exposing a larger fraction of the backbone to bond cleavage. See, for example D.M. Horn, Y. Ge, F.W. McLafferty, *Analytical Chemistry* 72 (2000) 4778–4784.
- [59] Breuker and co-workers also showed how increasing the charge state of a large peptide can expose a higher fraction of backbone residues to ECD cleavage presumably by disrupting the secondary structure (e.g., folding, α helices, salt bridges) of the peptide K. Breuker, S. Brüscheiler, M. Tollinger, *Angewandte Chemie International Edition* 50 (2011) 873–877.